

# Substoichiometric Molybdenum Sulfide Phases with Catalytically Active Basal Planes

Yang Bao,<sup>†,‡,§,▽</sup> Ming Yang,<sup>§,||,▽</sup> Sherman Jun Rong Tan,<sup>†,‡</sup> Yan Peng Liu,<sup>†</sup> Hai Xu,<sup>†</sup> Wei Liu,<sup>†,‡,§</sup> Chang Tai Nai,<sup>†</sup> Yuan Ping Feng,<sup>§,⊥</sup> Jiong Lu,<sup>†,§</sup> and Kian Ping Loh<sup>\*,†,§</sup>

<sup>†</sup>Department of Chemistry, National University of Singapore, Singapore 117543, Singapore

<sup>‡</sup>NUS Graduate School for Integrative Sciences and Engineering, National University of Singapore, Singapore 117456, Singapore

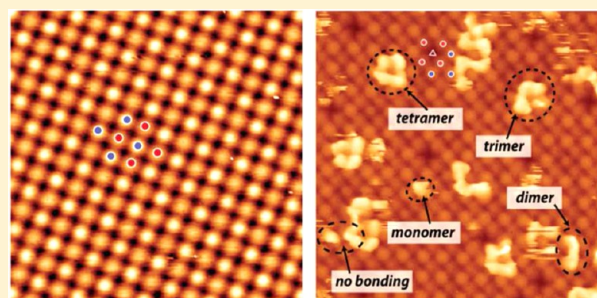
<sup>§</sup>Center for Advanced 2D Materials and Graphene Research Center, National University of Singapore, Singapore 117546, Singapore

<sup>||</sup>Institute of Materials Research and Engineering, Agency for Science, Technology and Research, Singapore 117602, Singapore

<sup>⊥</sup>Department of Physics, National University of Singapore, Singapore 117551, Singapore

## Supporting Information

**ABSTRACT:** Molybdenum sulfide ( $\text{MoS}_2$ ) is widely recognized for its catalytic activities where the edges of the crystals turn over reactions. Generating sulfur defects on the basal plane of  $\text{MoS}_2$  can improve its catalytic activity, but generally, there is a lack of model systems for understanding metal-centered catalysis on the basal planes. Here, we synthesized a new phase of substoichiometric molybdenum sulfide ( $s\text{-MoS}_x$ ) on a sulfur-enriched copper substrate. The basal plane of  $s\text{-MoS}_x$  contains chemically reactive Mo-rich sites that can undergo dynamic dissociative adsorption/desorption processes with molecular hydrogen, thus demonstrating its usefulness for hydrogen-transfer catalysis. In addition, scanning tunneling microscopy was used to monitor surface-directed Ullmann coupling of 2,8-dibromo-dibenzothiophene molecules on  $s\text{-MoS}_x$  nanosheets, where the 4-fold symmetric surface sites on  $s\text{-MoS}_x$  direct C–C coupling to form cyclic tetramers with high selectivity.



## INTRODUCTION

Molybdenum–sulfur compounds are widely recognized as an important class of non-noble metal catalysts. For example, alumina-supported molybdenum sulfides are important industrial catalysts in hydrosulfurization (HDS) processes.<sup>1</sup> Recently, molybdenum sulfide species in the molecular ( $\text{CP}_2\text{Mo}_2\text{S}_4$ ,  $\text{Mo}_3\text{S}_4^{4+}$ ,  $\text{Mo}_3\text{S}_{13}^{2-}$ , etc.),<sup>2–4</sup> nanoparticle,<sup>5,6</sup> or amorphous ( $\text{MoS}_2$ ,  $\text{MoS}_x$ )<sup>7,8</sup> forms have emerged as efficient catalysts in hydrogen evolution reactions (HER). For more effective Mo–S catalysts to be designed, fundamental insights on the nature of the active sites and the reaction mechanisms are needed. In view of the complexity of industrial catalysts, the study of catalyst operation is often undertaken with model systems on which surface characterization techniques are applied to interrogate the adsorption of molecular species on catalytic sites. Among the characterization techniques, scanning tunneling microscopy (STM) is particularly informative because it allows imaging of the active sites and active site–reactant interaction with atomic resolution.

Besenbacher and co-workers have pioneered the STM studies of substrate-supported  $\text{MoS}_2$ , which was used as a model system to understand catalytic activity on coordinatively unsaturated Mo edge sites.<sup>9–13</sup> Substoichiometric  $\text{MoS}_x$  ( $x < 2$ ) phases containing sulfur vacancies should be highly active for catalysis. Defect engineering of  $\text{MoS}_2$  was recently used to

activate its basal planes in HER, where improved activities are attributed to sulfur vacancies on the basal planes.<sup>14–17</sup> Industrial catalysts are prepared by partially converting substrate-supported molybdenum oxides to the sulfidic state, suggesting the existence of substoichiometric phases.<sup>18–20</sup> It is highly desirable to prepare simplified model catalysts that can imitate complex substoichiometric Mo–S compounds, where insights on the catalyst operation and preparation can be obtained. Conceptually, it is possible to grow substrate-stabilized phases of molybdenum sulfides ( $s\text{-MoS}_x$ ) because the interfacial stabilization allows greater flexibility in bonding configurations; thus, sulfide phases with unique structures and catalytic properties can be created. Recently, substrate-stabilized molybdenum sulfide structures have been prepared on Cu(111) and graphite, including  $\text{Mo}_6\text{S}_6$  nanowires<sup>21,22</sup> and  $\text{Mo}_2\text{S}_3$  islands.<sup>23</sup>

Herein, a new molybdenum sulfide ( $s\text{-MoS}_x$ ) phase was prepared on sulfur-enriched Cu(111), which can serve as a good Mo–S model catalyst for fundamental catalytic studies. In situ STM reveals the existence of alternating Mo- and S-rich sites in a square lattice on the basal plane of  $s\text{-MoS}_x$ , although the exact structure cannot be determined at this stage. The

Received: August 31, 2016

Published: October 3, 2016

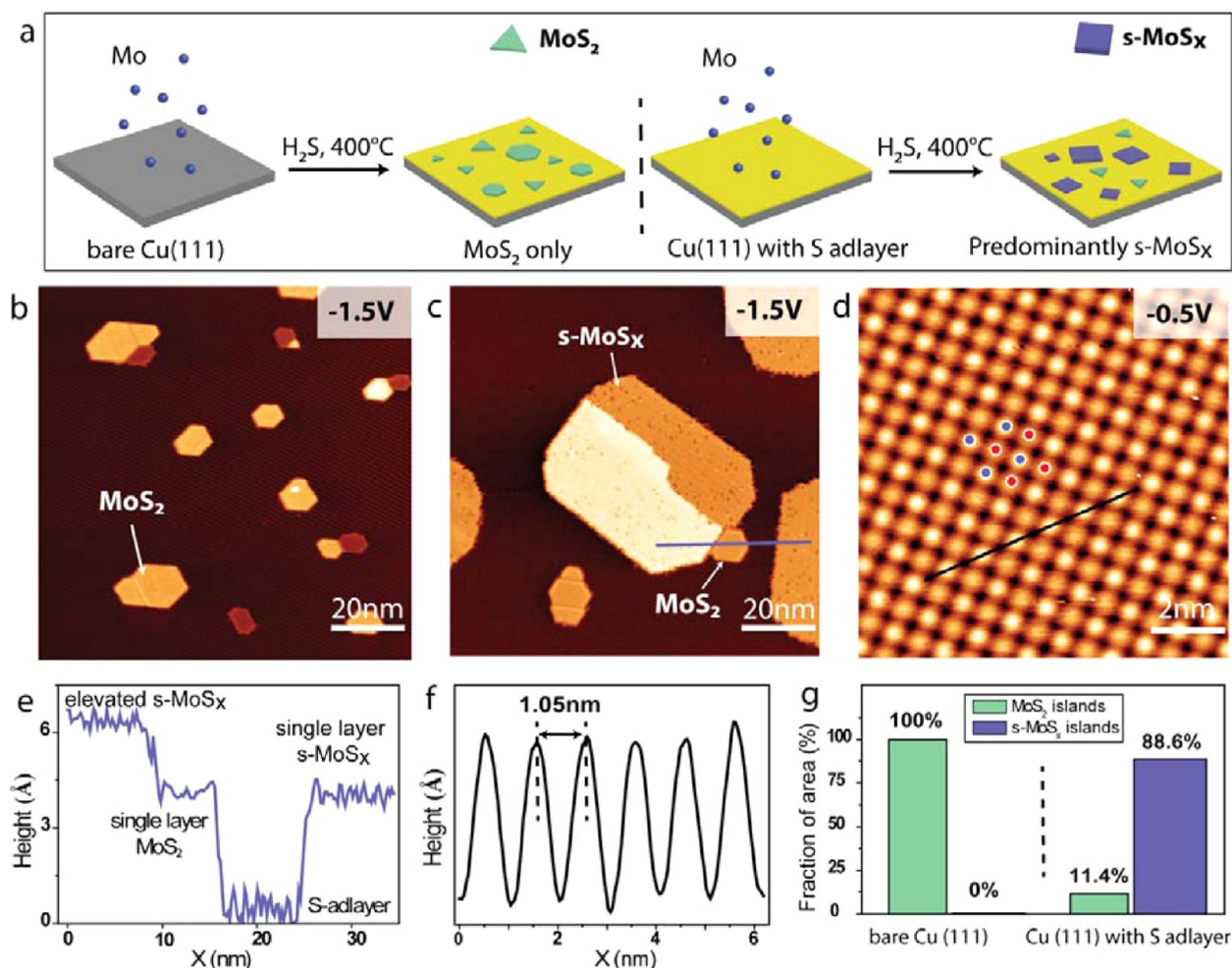


**Figure 1.** Preparation of  $s\text{-MoS}_x$ . (a) Schematic illustration of two different growth methods for selective preparation of  $\text{MoS}_2$  and  $s\text{-MoS}_x$ . (b) STM image of substrate surface containing only  $\text{MoS}_2$  islands. Scale bar, 20 nm. (c) STM image of an  $s\text{-MoS}_x$  island-dominated surface with a minority of small  $\text{MoS}_2$  islands. Scale bar, 20 nm. (d) High-resolution STM image of the  $s\text{-MoS}_x$  surface. Two different surface sites are marked by red and blue dots. Scale bar, 2 nm. (e) STM height profile along a line marked in c to measure the heights of islands. (f) STM height profile along a line marked in d to measure the surface site periodicity. (g) Relative surface coverage of  $\text{MoS}_2$  and  $s\text{-MoS}_x$  islands on samples prepared on bare Cu(111) and Cu(111) with S adlayer, respectively.

highly reactive Mo-rich sites on the basal plane interact strongly with molecular hydrogen to form well-defined hydrogen adsorption patterns that are thermally stable below 200 °C. We also studied the interaction of  $s\text{-MoS}_x$  with 2,8-dibromodibenzothiophene (DBDBT) molecules to demonstrate the wide applicability of the model catalytic system toward C–C coupling reactions. STM studies show that the 4-fold symmetric Mo-rich sites allow the adsorptive preassembly of DBDBT molecules and catalyze Ullmann type aryl–aryl coupling to form cyclic tetramers with high selectivity.

## EXPERIMENTAL SECTION

**Sample Preparation.** Experiments were performed in an ultrahigh vacuum chamber (UHV, base pressure of  $10^{-10}$  mbar) with a UHV STM unit (high-temperature STM 150 Aarhus, SPECS, GmbH). The Cu(111) substrate (Mateck, GmbH) was cleaned by repeated argon ion sputtering at  $p(\text{Ar}) = 1 \times 10^{-5}$  mbar, 1.5 keV, followed by annealing at 600 °C. Growth of  $\text{MoS}_2$  or  $s\text{-MoS}_x$  islands were carried out by evaporating Mo atoms onto the substrates, followed by annealing in  $\text{H}_2\text{S}$  at elevated temperatures (400–700 °C).

**Interaction of  $s\text{-MoS}_x$  with  $\text{H}_2$  and  $\text{O}_2$ .** The hydrogenation experiment was performed by dosing  $\text{H}_2$  at  $1 \times 10^{-6}$  mbar while keeping the sample at temperatures ranging from room temperature to

80 °C. Hydrogen desorption was performed by annealing the hydrogenated sample at 200 °C in vacuum. The oxygenation experiment was performed by dosing  $\text{O}_2$  at  $1 \times 10^{-6}$  mbar while keeping the sample at room temperature.

**Interaction of  $s\text{-MoS}_x$  with DBDBT.** 2,8-Dibromodibenzothiophene (DBDBT) molecules with 96% purity (Tokyo Chemical Industry Co., Ltd.) were dosed with a Knudsen cell (MBE-Komponenten, GmbH) at 48 °C. After deposition, oligomerization of DBDBT was induced by annealing the sample at 200 °C.

**X-ray Photoelectron Spectroscopy (XPS) Studies.** XPS characterizations were carried out using a SPECS XR 50 X-ray Mg  $K\alpha$  (1486.6 eV) source with pass energy of 30 eV, PHOIBOS 150 hemispherical energy analyzer (SPECS, GmbH), and a 3-D delay line detector (SPECS, GmbH) with a base pressure of  $5 \times 10^{-10}$  mbar. The binding energies of the XPS spectra were calibrated to the Au  $4f_{7/2}$  peaks. XPS peak fitting was carried out using a mixed Gaussian–Lorentzian function after Shirley background subtraction. An area ratio of 3:2 between the Mo  $3d_{5/2}$  and  $3d_{3/2}$  peaks and an area ratio of 2:1 between the S  $2p_{3/2}$  and  $2p_{1/2}$  peaks were employed in the fitting with the same full width at half maximum (fwhm). The spin–orbit splitting for Mo 3d and S 2p spectra are 3.2 and 1.2 eV, respectively.

## RESULTS AND DISCUSSION

**Preparation of  $s\text{-MoS}_x$ .** Molybdenum sulfide islands were prepared by evaporating submonolayer Mo atoms onto the substrate followed by sulfurization in  $\text{H}_2\text{S}$  ( $1 \times 10^{-6}$  mbar) at elevated temperatures (Figure 1a). On a clean Cu(111) surface, this process leads to the formation of  $\text{MoS}_2$  with hexagonal or truncated triangular morphologies (see Figure 1b), similar to previously reported works.<sup>24</sup> However, if the Cu(111) surface is sulfurized first to form the well-known ( $\sqrt{7} \times \sqrt{7}$ )  $R 19^\circ$  Cu–S adlayer<sup>25</sup> (see Supplementary Figure 1a) before the evaporation of binary atomic sources, a structurally different compound, denoted as  $s\text{-MoS}_x$ , is formed in reasonably high yield. Single-layer (apparent height of 3.5 Å) islands and elevated domains (apparent height of 6.5 Å) of  $s\text{-MoS}_x$  with truncated rectangular shapes are observed (Figure 1c and e). The elevated domains could be attributed to bilayer growth or buried Cu adatoms beneath the  $s\text{-MoS}_x$  islands, which we cannot distinguish with certainty here.<sup>24</sup> A high-resolution STM image of the  $s\text{-MoS}_x$  surface (Figure 1d) revealed two types of bright spots with different contrast (marked by red and blue dots), which we interpret as two different surface sites. Bright spots of the same type form a square array with a periodicity of 1.05 nm (Figure 1f). STM spectroscopy shows that  $s\text{-MoS}_x$  also has a different electronic structure from that of  $\text{MoS}_2$  (see Supplementary Figure 2).

We notice that sulfur-enrichment of the substrate is crucial for the preferential formation of  $s\text{-MoS}_x$  islands. Typically, the Cu(111) substrate is annealed in  $\text{H}_2\text{S}$  at 400 °C for 1 h to form a fully covered Cu–S adlayer; then,  $s\text{-MoS}_x$  nanosheets with a high surface coverage (Supplementary Figure 1b) can be grown by annealing as-deposited Mo in  $\text{H}_2\text{S}$  at 600 °C for 20 min. The S-enriched substrate most likely provides interfacial stabilization for  $s\text{-MoS}_x$  with its Mo-rich surface sites supported by the row-matching registry of the  $s\text{-MoS}_x$  overlayer with the Cu–S substrate (see Supplementary Figure 3 for detailed discussion of the row-matching registry). It is difficult to maintain complete coverage of the Cu–S adlayer at the growth temperature used due to the diffusion of highly mobile  $\text{Cu}_3\text{S}_3$  clusters.<sup>26,27</sup> This process inevitably exposes bare Cu regions on the substrate, where the growth of  $\text{MoS}_2$  is favored; thus, typically approximately 10% of  $\text{MoS}_2$  and 90% of  $s\text{-MoS}_x$  islands coexist on the surface (Figure 1g). We also observed that, with increased annealing time or temperature, the surface coverage of  $\text{MoS}_2$  increases while that of the  $s\text{-MoS}_x$  decreases; these are the consequences of thermally induced disruption of the Cu–S adlayer, which are essential for supporting the  $s\text{-MoS}_x$  phase.

**Characterization of the  $s\text{-MoS}_x$  Phase.** STM studies reveal that the surface lattice of the  $s\text{-MoS}_x$  phase has a square symmetry, which is markedly different from the hexagonal symmetry of the  $\text{MoS}_2$  lattice. At negative sample biases, where electrons tunnel from the sample to the tip,<sup>28</sup> local filled states of the two surface sites (marked by red and blue dots) are imaged as bright spots with 4-fold symmetry (Figure 2a). At positive sample biases, which image the local empty states, only the sites marked by red dots are imaged as bright spots (Figure 2b). In  $\text{MoS}_2$  and  $\text{Mo}_6\text{S}_6$ , empty states originate almost exclusively from the Mo d orbitals, whereas the filled states are contributed by both the Mo and S orbitals.<sup>21,29</sup> This can be understood as the electron density is polarized toward the more electronegative sulfur atoms, rendering the empty states to be located at the metal atoms. We infer that Mo atoms are the

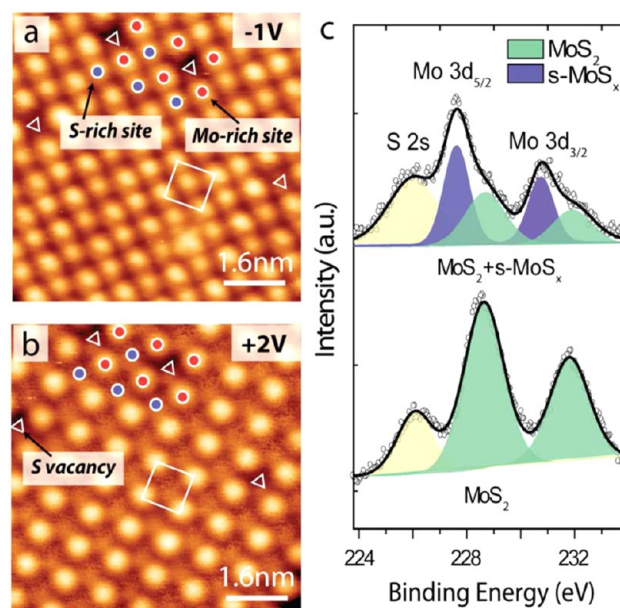


**Figure 2.** Characterization of  $s\text{-MoS}_x$ . (a,b) Filled- and empty-state STM images taken at  $-1$  and  $+2$  V of the same area. Mo-rich sites, red dots; S-rich sites, blue dots; defect sites, hollow triangles. White squares representing individual unit cells were superimposed onto the two images. Scale bar, 1.6 nm. (c) Deconvolution of the XPS spectra reveals chemically shifted Mo 3d peaks (in blue) assignable to  $s\text{-MoS}_x$ . The Mo 3d peaks from  $\text{MoS}_2$  are labeled in green, and the S 2s peak is labeled in yellow.

reactive metal species on the surface because XPS spectra of oxygen-exposed  $s\text{-MoS}_x$  revealed peaks assignable to molybdenum oxysulfide but no signals from oxidized Cu. In addition, we obtained evidence for the dissociative adsorption of molecular hydrogen on the surface of  $s\text{-MoS}_x$ , a reaction likely to be catalyzed by the highly reactive Mo atoms rather than the Cu atoms (see discussion in the succeeding section). In this case, we assign the sites marked by red dots to the Mo-rich sites, and the sites marked by blue dots to the S-rich sites. The bias-dependent contrast of the two surface sites is further illustrated in Supplementary Figure 4. We also observed the presence of defect sites on the  $s\text{-MoS}_x$  surface (see Supplementary Figure 5), which coincide with where the S-rich sites were, suggesting that these are S vacancies (hollow triangles in Figure 2a and b).

The chemical states of elements in  $s\text{-MoS}_x$  were studied by XPS. Comparing the XPS spectra of the  $\text{MoS}_2$  and the  $s\text{-MoS}_x$  dominated samples, it can be seen that the  $s\text{-MoS}_x$  dominated sample presents a chemically shifted Mo 3d peak at 227.6 eV (Figure 2c). The binding energy is approximately 1 eV lower than that of the Mo atoms (+4) in  $\text{MoS}_2$ , indicating an intermediate oxidation state of +2 or +3.<sup>30</sup> The XPS spectra of S 2p peaks show that sulfur atoms in both samples have the same  $-2$  oxidation state (see Supplementary Figure 6). On the basis of the chemical states of Mo and S atoms, we can infer that  $s\text{-MoS}_x$  is substoichiometric. However, we cannot resolve the full atomic structure of  $s\text{-MoS}_x$  at this stage, as it is difficult to delaminate the nanosheets from the substrate for ex situ diffraction studies. Nonetheless, a plausible  $\text{Mo}_{18}\text{S}_{18}$  structure was proposed based on combined surface characterization and density functional theory (DFT) studies (see Supplementary Figure 7).

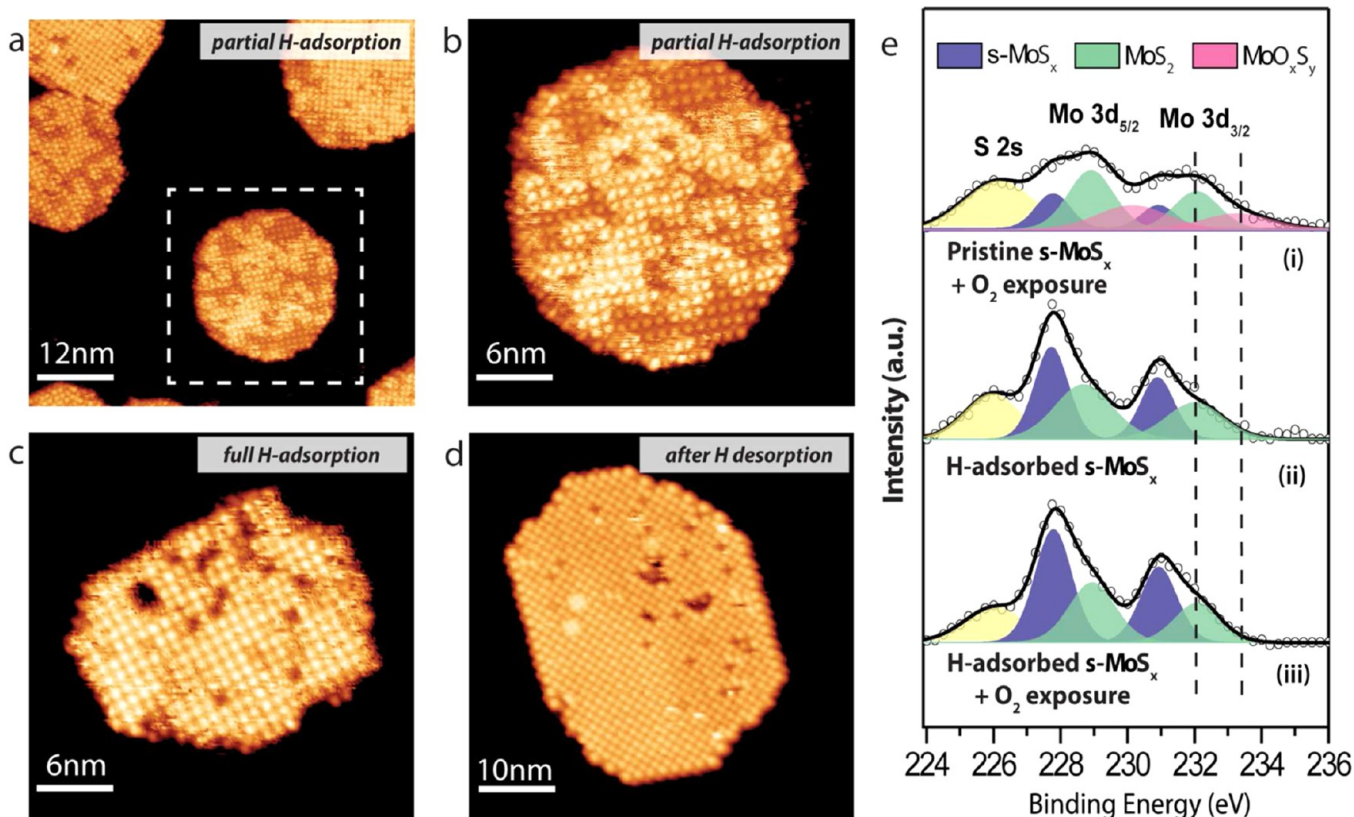


**Figure 3.** Hydrogen passivation of  $s\text{-MoS}_x$ . (a) STM image of hydrogen adlayer on  $s\text{-MoS}_x$  formed at 80 °C. Scale bar, 12 nm. (b) Magnified STM image of the area marked in a, where the bright spots with 4-fold symmetry and  $\sim 1$  nm periodicity are patterns observed after hydrogen adsorption. Scale bar, 6 nm. (c) STM image of an  $s\text{-MoS}_x$  island with fully covered hydrogen adlayer. Scale bar, 6 nm. (d) STM image of one  $s\text{-MoS}_x$  island regenerated after the hydrogen adsorption-oxygen exposure-hydrogen desorption cycle. Scale bar, 10 nm. (e) XPS spectra of  $s\text{-MoS}_x$  with hydrogen adsorption (spectrum ii), and the same sample after oxygen exposure (spectrum iii); there is no observable shift in the Mo binding energies. In contrast, XPS spectrum of pristine  $s\text{-MoS}_x$  exposed to oxygen (spectrum i) reveals an additional set of Mo 3d peaks at higher binding energies, which is assignable to molybdenum oxysulfide.<sup>31</sup> Typical XPS spectrum for pristine  $s\text{-MoS}_x$  is given in Figure 2c.

**Interaction of  $s\text{-MoS}_x$  with Small Gas Molecules.** To test the reactivity of  $s\text{-MoS}_x$ , we first introduced oxygen ( $1 \times 10^{-6}$  mbar) into the UHV chamber for 1 h while keeping the sample at room temperature. After oxygen exposure,  $s\text{-MoS}_x$  was rapidly oxidized in a destructive and irreversible manner, as judged by its corroded basal plane in the STM images (see Supplementary Figure 8), and the appearance of a high binding energy Mo 3d<sub>5/2</sub> peak at 230.2 eV in XPS (spectrum i in Figure 3e), which is assignable to molybdenum oxysulfide phases.<sup>31</sup> XPS spectrum of the Cu 2p (see Supplementary Figure 9) and S 2p core level peaks show no detectable changes, suggesting that (1) S atoms in  $s\text{-MoS}_x$ ,  $\text{MoS}_2$ , and the Cu–S adlayer do not react with oxygen at room temperature and that (2) the Cu atoms in  $s\text{-MoS}_x$ , if any, are not exposed at the surface. Although the chemical shift of surface Cu species could be masked by a large Cu background from the substrate, these results suggest the  $s\text{-MoS}_x$  surface contains undercoordinated Mo atoms that are chemically reactive.

Interestingly, we observed that hydrogen molecules are dissociatively adsorbed on the  $s\text{-MoS}_x$  basal plane, passivating it from oxidation, and the catalytic sites can be reactivated dynamically following hydrogen desorption. STM revealed that room temperature adsorption of  $\text{H}_2$  results in a fuzzy-looking film on  $s\text{-MoS}_x$  islands (see Supplementary Figure 10). Intriguingly, if the sample is heated to 80 °C while dosing  $\text{H}_2$  for 15 min, a highly ordered hydrogen adlayer with 4-fold symmetry and a periodicity of approximately 1 nm is formed on

the surface (Figure 3a and b and Supplementary Figure 11). Typically, a fully covered hydrogen adlayer on  $s\text{-MoS}_x$  can be achieved after a long exposure time of 1 h (Figure 3c).

The fact that a clear hydrogen adsorption pattern can be imaged by room-temperature STM suggests a relatively strong interaction of adsorbed hydrogen with the substrate, which can be ascribed to atomic hydrogen rather than molecular dihydrogen because the imaging of physisorbed  $\text{H}_2$  at room temperature has never been achieved due to its very weak binding. On the other hand, chemisorbed atomic hydrogen is stable enough to be imaged by STM at room temperature.<sup>32,33</sup> The different stabilities of physisorbed and chemisorbed hydrogen is also reflected in temperature-programmed desorption (TPD) studies on metal surfaces. For reactive metals such as Pd, desorption of physisorbed hydrogen occurs at very low temperature (below 100 K), whereas chemisorbed atomic hydrogen desorbs at much higher temperatures (100–400 K).<sup>34</sup>

On the basis of the proposed  $\text{Mo}_{18}\text{S}_{18}$  model, the most energetically stable hydrogen adsorption configuration was identified; the binding of hydrogen on top of the Mo atom gives an adsorption energy of  $-0.28$  eV (exothermic), which is much larger than the typical physical adsorption energies ranging from  $-0.01$  to  $-0.1$  eV (see Supplementary Figure 12).<sup>35</sup> The calculated adsorption energy reflects the chemical reactivity of undercoordinated Mo atoms in Mo–S structural motifs. It should be noted that compounds such as  $\text{Mo}(100)$ <sup>36</sup>

and molybdenum carbide<sup>37</sup> are very reactive toward hydrogen chemisorption, partly due to the incomplete filling of the Mo d-orbitals.<sup>38,39</sup> On the other hand, group 11 elements (Cu, Ag, and Au) with fully occupied d-orbitals are known to be relatively inert.<sup>38</sup> For example, the hydrogen adsorption energy on single crystalline Cu(111) is around +0.03 eV (endothermic).<sup>39</sup> Therefore, the ordered hydrogen adlayer observed by STM is attributed to chemisorbed hydrogen on surface Mo atoms. This result suggests that coordinatively unsaturated Mo atoms in Mo–S species might play a pivotal role in activating molecular hydrogen, whereas previous studies on HER catalysts have mainly focused on the adsorption of hydrogen on sulfur sites.<sup>2,4,8,40,41</sup> Very recently, Artero and co-workers revisited the HER catalytic mechanism for amorphous molybdenum sulfide (a-MoS<sub>x</sub>).<sup>42</sup> The authors found that molybdenum-hydride moieties are the active sites under H<sub>2</sub> evolution conditions, which is consistent with our insight that it is the unsaturated Mo atoms, rather than the S atoms, that interact strongly with hydrogen.

The hydrogen adsorbed s-MoS<sub>x</sub> sample is analyzed by XPS to examine the different bonding states. Unlike oxidation-induced peak shifts, there are no detectable chemical shifts in Mo 3d or S 2p core level peaks upon hydrogenation, suggesting that charge transfer between adsorbed hydrogen and the active site, if any, is weak (spectrum ii in Figure 3e). The hydrogen adsorbed s-MoS<sub>x</sub> nanosheets were also exposed to O<sub>2</sub> (1 × 10<sup>-6</sup> mbar) at room temperature for 1 h. Following this, no observable changes in the Mo 3d or S 2p core level peaks were observed (spectrum iii in Figure 3e), suggesting that surface Mo atoms are chemically passivated by the hydrogen adlayer. The clean s-MoS<sub>x</sub> sample can be regenerated after annealing it at 200 °C, as judged from the regeneration of smooth basal planes in STM images (Figure 3d). The ability of s-MoS<sub>x</sub> to undergo dynamic adsorption/desorption with molecular hydrogen suggests its potential as a model catalytic system for the mechanistic study of hydrogen-transfer reactions, e.g., hydrogenation or hydrodesulfurization.

#### Interaction of s-MoS<sub>x</sub> with Organic Molecules.

Ullmann coupling has attracted increasing attention recently due to its wide application in the synthesis of functional macromolecular systems, including polymeric chains,<sup>43,44</sup> graphene nanoribbons,<sup>45</sup> and covalently linked molecular frameworks.<sup>46</sup> Because of the presence of Mo-rich sites, s-MoS<sub>x</sub> potentially shows reactivity toward nucleophilic molecules such as 2,8-dibromo-dibenzothiophene (DBDBT), which has lone pair electrons located at the S atom. DBDBT has two bromine functional groups; thus, it can undergo polymerization via the Ullmann coupling reaction after debromination.

As-deposited molecules are highly diffusive at room temperature when subjected to tip–sample interactions, making it challenging to obtain high quality STM images. After mild annealing at 80 °C, individual DBDBT molecules can be readily imaged by STM and appear as bright protrusions on the surface of s-MoS<sub>x</sub> (Figure 4, Supplementary Figures 13 and 14a). In contrast, the surfaces of MoS<sub>2</sub> and Cu–S remain almost free of molecules (see Supplementary Figure 14b), probably because these two surfaces are coordinatively saturated. Using the S vacancy site as a surface marker, the s-MoS<sub>x</sub> surface sites can be identified as either Mo- or S-rich sites (marked by red and blue dots, respectively, in Figure 4c). We observed that bright protrusions corresponding to DBDBT molecules coincide with where the Mo-rich sites were. This is expected as the Mo-rich sites present unoccupied states near the Fermi level, which may

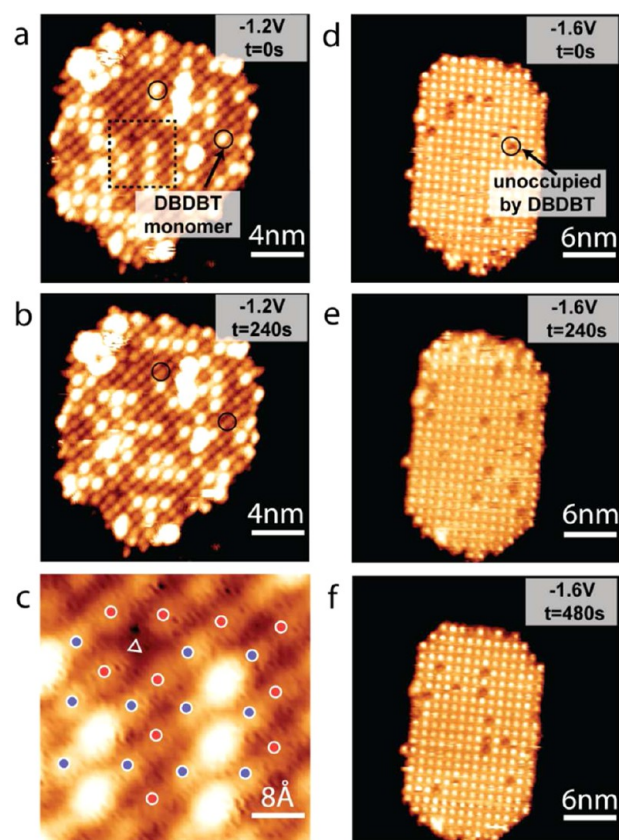


**Figure 4.** DBDBT adsorption on s-MoS<sub>x</sub>. (a, b) STM images recorded consecutively at 0 and 240 s of one s-MoS<sub>x</sub> island partially covered by DBDBT molecules. Each bright protrusion corresponds to one DBDBT molecule. The hollow circles mark two representative surface sites where adsorbed molecules diffused away. Scale bar, 4 nm. (c) Magnified STM image of the area marked in a, where DBDBT molecules adsorb exclusively on the Mo-rich sites. Mo-rich sites, red dots; S-rich sites, blue dots; defect sites, hollow triangles; Scale bar, 8 Å. (d–f), STM images of one s-MoS<sub>x</sub> island with near-full coverage of DBDBT molecules recorded consecutively at 0, 240, and 480 s. The dark spots correspond to surface sites on s-MoS<sub>x</sub> that are not occupied by DBDBT molecules. The dark spots constantly change in position due to the constant migration of DBDBT molecules in the adlayer.

be occupied by lone pair electrons from the sulfur atoms in DBDBT molecules. In two STM images recorded consecutively at the same area (Figure 4a and b), molecules were found to migrate to different Mo-rich sites, suggesting a relatively weak interaction (i.e., Molybdenum–sulfur coordination) between DBDBT and the Mo-rich sites. In the high surface coverage regime, DBDBT molecules form a 4-fold symmetric adlayer on the surface of s-MoS<sub>x</sub> with a similar appearance to the hydrogen adlayer (Figure 4d–f). The dark spots in the molecular film correspond to surface sites on s-MoS<sub>x</sub> that are not occupied by DBDBT. In STM images taken with temporal resolution, it is observed that the dark spots in the adlayer constantly migrate (Figure 4d–f), which can be explained by the constant migration of molecules to their adjacent unoccupied surface sites.

Oligomerization was induced by annealing the as-deposited molecules at 200 °C; thereafter, short-chain oligomers were formed exclusively on the surface of s-MoS<sub>x</sub>, whereas the MoS<sub>2</sub> and Cu–S surfaces remained unreacted with the molecules (Figure 5a and Supplementary Figure 15). This presents strong evidence that basal planes of s-MoS<sub>x</sub> are catalytically active. It is

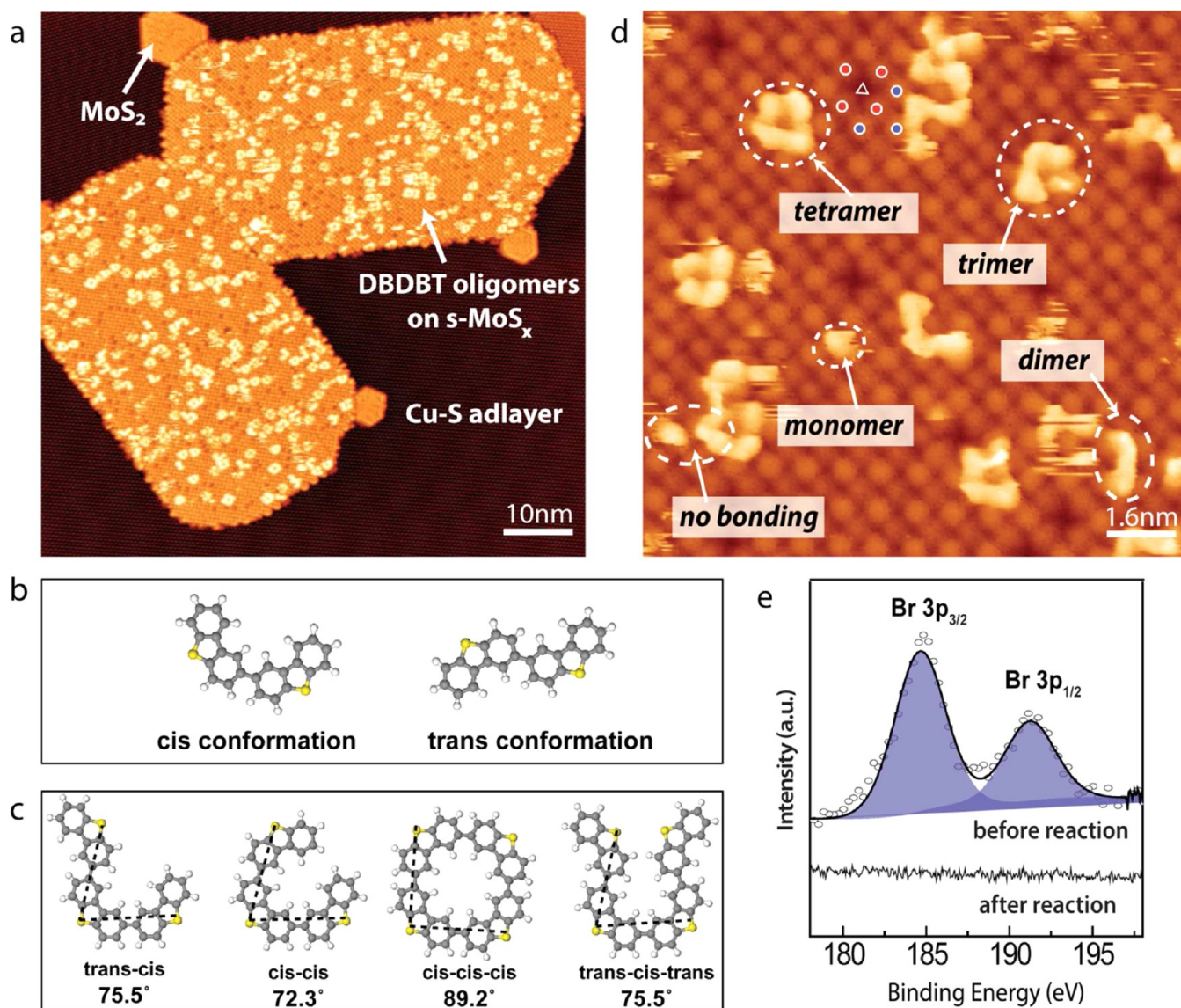


**Figure 5.** DBDBT oligomerization on *s*-MoS<sub>x</sub> in the low surface coverage regime. (a) STM image of *s*-MoS<sub>x</sub> islands adsorbed with DBDBT oligomers. Scale bar, 10 nm. (b) Neighboring DBDBT monomers can only adopt two possible conformations: cis or trans. (c) Structural models of DBDBT trimers and tetramers based on the combination of local cis and trans conformations with the distance between neighboring sulfur atoms being 1.1 nm and the angles labeled in the figure. (d) Magnified STM image of DBDBT oligomers on the surface of *s*-MoS<sub>x</sub>. Surface molecular species ranging from monomer to tetramer, as well as the nonbonding regime between adjacent molecular species, are marked accordingly. Mo-rich sites are marked by red dots, and S-rich sites are marked by blue dots. (e) XPS spectrum of as-deposited DBDBT molecules on *s*-MoS<sub>x</sub> gives rise to Br 3p core level peaks; after annealing the sample at 200 °C for 1 h, no signal of the Br 3p peaks can be observed, indicating the successful cleavage of C–Br bonds and desorption of Br atoms.

noteworthy that typical reaction temperatures for Ullmann coupling on catalytic metal substrates are around 200 °C.<sup>43–46</sup> The oligomer conformation arises from various linear combinations of local cis or trans conformations between two neighboring monomer residues, where the cis conformation refers to the sulfur atoms located on the same side of the aromatic backbone and the trans conformation refers to the sulfur atoms on the opposite side (Figure 5b). Oligomerization product in the simplest form, i.e., the dimer, has only two possible conformations. Structural models of some simple trimers and tetramers are given in Figure 5c. Calculations show that, in all conformations, the S–S distance of two neighboring units is around 1.1 nm, whereas the S–S angles vary considerably. The local cis conformation gives a S–S angle of 72.3°, and the local trans conformation gives a S–S angle of

75.5°. However, if cyclic oligomers were formed, a large deviation in the S–S angle should be expected due to the rigidity of the enclosed aromatic backbone. Such strained structure can be supported, however, if the substrate can immobilize individual monomers.

In the low coverage regime of DBDBT molecules on *s*-MoS<sub>x</sub>, a random distribution of molecular species was observed after thermally induced oligomerization. Figure 5d shows various forms of molecular species ranging from monomer to tetramer. The occurrence of covalent bonding can be unambiguously discerned by the bright features between adjacent monomer units, which reflect enhanced density of states originating from the overlapped C sp<sup>2</sup> orbitals. In contrast, there is an obvious gap between adjacent molecular species (no bonding site marked in Figure 5d), indicating the absence of shared orbitals.

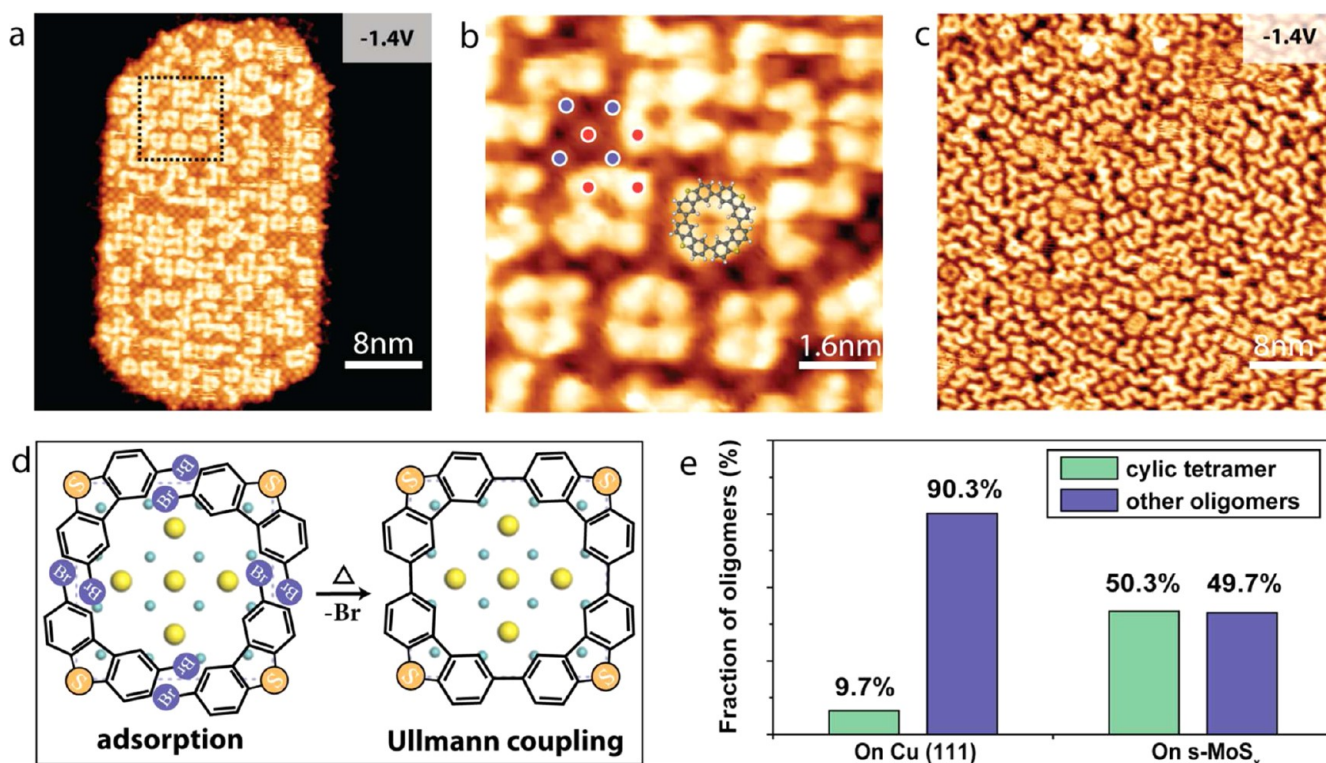


**Figure 6.** DBDBT oligomerization on  $s\text{-MoS}_x$  in the high surface coverage regime. (a) STM image of one  $s\text{-MoS}_x$  island with a high coverage of DBDBT oligomers. Scale bar, 8 nm. (b) Magnified STM image of the area marked in a; the structural model of the cyclic tetramer is superimposed on the image. Scale bar, 1.6 nm. Mo-rich sites, red dots; S-rich sites, in blue dots. (c) STM image of DBDBT oligomers formed on Cu(111) with disordered shapes and orientations. Scale bar, 8 nm. (d) Schematic illustration of the possible reaction mechanism, where the debromination of preassembled DBDBT molecules leads to selective formation of cyclic tetramers. (e) Statistics of cyclic tetramers formed on Cu(111) and  $s\text{-MoS}_x$ .

The occurrence of reaction is also supported by the changes in Br 3p peaks in the XPS spectra (Figure 5e).

In the high surface coverage regime of DBDBT molecules on  $s\text{-MoS}_x$ , it is observed that the oligomers tend to form cyclic tetramers (see Figure 6a and b). This could be explained by the local connection of preassembled DBDBT radicals on the Mo-rich sites, which have an intrinsic 4-fold symmetry. A successful template-directed assembly allows the preassembled structures formed by reactants to be inherited by the polymerization products. For example, Lin et al. used Cu-pyridyl coordination to preassemble reactants into linear chains, which serve as a template for subsequent Ullmann coupling to occur in a line-by-line fashion.<sup>43</sup> Herein, at high coverage regime, DBDBT molecules are preassembled into a  $1.05\text{ nm} \times 1.05\text{ nm}$  square array on the surface Mo-rich sites via Mo–S coordination. Upon thermal activation, these molecules couple readily to form cyclic tetramers (Figure 6d), where the S–S distance of two neighboring units is 1.1 nm and the internal angle of the enclosed cycle is  $89.2^\circ$  (see Figure 5c), which matches the square-lattice of the  $s\text{-MoS}_x$  surface. Indeed, the aromatic backbones of cyclic tetramers are found to align with the surface Mo-rich sites (Figure 6b). Control experiment for the polymerization of DBDBT molecules on Cu(111), which is a well-known metal catalyst for Ullmann coupling, produces randomly arranged oligomers with inhomogeneous shapes (Figure 6c and Supplementary Figure 16). The product distribution is obtained by counting the number of molecular species in the STM images acquired at different areas (see Supplementary Figure 17), which reveals a 50.3% selectivity for cyclic tetramers among all oligomers on  $s\text{-MoS}_x$ , a 5-fold

increase compared to the 9.7% selectivity on Cu(111) (Figure 6e).

## CONCLUSIONS

We report the preparation of a new substoichiometric  $s\text{-MoS}_x$  phase on sulfur-enriched Cu(111) surface. In contrast to the catalytically inactive basal plane of  $\text{MoS}_2$ , the Mo-rich sites on the basal plane of  $s\text{-MoS}_x$  are chemically reactive and afford a model system for investigating metal-centered catalysis. STM studies showed that hydrogen molecules adsorb dissociatively on Mo-rich sites and can undergo dynamic adsorption and desorption at elevated temperatures; thus,  $s\text{-MoS}_x$  can be used as a hydrogen-transfer catalyst. Ullmann coupling of DBDBT molecules, catalyzed by the basal planes of  $s\text{-MoS}_x$ , was also observed; its 4-fold symmetric surface sites direct the C–C coupling of DBDBT to form cyclic tetramers with high selectivity. Finally, our work hints at the possibility of other substoichiometric phases of transition metal chalcogenides with rich physical and chemical properties and that different substrates may support specific substoichiometric phases with distinct crystal structures and surface properties.

## ASSOCIATED CONTENT

### Supporting Information

The Supporting Information is available free of charge on the ACS Publications website at DOI: 10.1021/jacs.6b09042.

Additional STM, STS, and XPS data for the characterization of  $s\text{-MoS}_x$ ; DFT calculations of the  $s\text{-MoS}_x$  structure; and additional STM, XPS, and DFT data for

s-MoS<sub>x</sub> interactions with gaseous and organic molecules  
(PDF)

## AUTHOR INFORMATION

### Corresponding Author

\*chmlohkp@nus.edu.sg

### Author Contributions

Y.B., M.Y., and S.J.R.T. contributed equally to this work.

### Notes

The authors declare no competing financial interest.

## ACKNOWLEDGMENTS

The authors acknowledge funding support from the Center for Advanced 2D Materials (CA2DM), NUS under the National Research Foundation (NRF) Mid-sized Center grant, Prime Minister's Office, Singapore. M.Y. thanks CA2DM for providing the computational resources and also the funding support from A\*-STAR 2D PHAROS project (Project No. 1527000012).

## REFERENCES

- (1) Topsøe, H.; Clausen, B. S. *Appl. Catal.* **1986**, *25*, 273.
- (2) Appel, A. M.; DuBois, D. L.; Rakowski DuBois, M. *J. Am. Chem. Soc.* **2005**, *127*, 12717.
- (3) Jaramillo, T. F.; Bonde, J.; Zhang, J.; Ooi, B.-L.; Andersson, K.; Ulstrup, J.; Chorkendorff, I. *J. Phys. Chem. C* **2008**, *112*, 17492.
- (4) Kibsgaard, J.; Jaramillo, T. F.; Besenbacher, F. *Nat. Chem.* **2014**, *6*, 248.
- (5) Walton, A. S.; Lauritsen, J. V.; Topsøe, H.; Besenbacher, F. *J. Catal.* **2013**, *308*, 306.
- (6) Asadi, M.; Kumar, B.; Behranginia, A.; Rosen, B. A.; Baskin, A.; Repnin, N.; Pisasale, D.; Phillips, P.; Zhu, W.; Haasch, R.; Klie, R. F.; Kral, P.; Abiade, J.; Salehi-Khojin, A. *Nat. Commun.* **2014**, *5*, 4470.
- (7) Tang, M. L.; Grauer, D. C.; Lassalle-Kaiser, B.; Yachandra, V. K.; Amirav, L.; Long, J. R.; Yano, J.; Alivisatos, A. P. *Angew. Chem., Int. Ed.* **2011**, *50*, 10203.
- (8) Lassalle-Kaiser, B.; Merki, D.; Vrabel, H.; Gul, S.; Yachandra, V. K.; Hu, X.; Yano, J. *J. Am. Chem. Soc.* **2015**, *137*, 314.
- (9) Lauritsen, J. V.; Kibsgaard, J.; Helveg, S.; Topsøe, H.; Clausen, B. S.; Laegsgaard, E.; Besenbacher, F. *Nat. Nanotechnol.* **2007**, *2*, 53.
- (10) Kibsgaard, J.; Clausen, B. S.; Topsøe, H.; Laegsgaard, E.; Lauritsen, J. V.; Besenbacher, F. *J. Catal.* **2009**, *263*, 98.
- (11) Tuxen, A.; Kibsgaard, J.; Göbel, H.; Laegsgaard, E.; Topsøe, H.; Lauritsen, J. V.; Besenbacher, F. *ACS Nano* **2010**, *4*, 4677.
- (12) Tuxen, A. K.; Führtbauer, H. G.; Temel, B.; Hinnemann, B.; Topsøe, H.; Knudsen, K. G.; Besenbacher, F.; Lauritsen, J. V. *J. Catal.* **2012**, *295*, 146.
- (13) Kibsgaard, J.; Tuxen, A.; Knudsen, K. G.; Brorson, M.; Topsøe, H.; Laegsgaard, E.; Lauritsen, J. V.; Besenbacher, F. *J. Catal.* **2010**, *272*, 195.
- (14) Li, H.; Tsai, C.; Koh, A. L.; Cai, L.; Contryman, A. W.; Fragapane, A. H.; Zhao, J.; Han, H. S.; Manoharan, H. C.; Abild-Pedersen, F.; Nørskov, J. K.; Zheng, X. *Nat. Mater.* **2016**, *15*, 48.
- (15) Xie, J.; Zhang, H.; Li, S.; Wang, R.; Sun, X.; Zhou, M.; Zhou, J.; Lou, X. W.; Xie, Y. *Adv. Mater.* **2013**, *25*, 5807.
- (16) Ouyang, Y.; Ling, C.; Chen, Q.; Wang, Z.; Shi, L.; Wang, J. *Chem. Mater.* **2016**, *28*, 4390.
- (17) Ye, G.; Gong, Y.; Lin, J.; Li, B.; He, Y.; Pantelides, S. T.; Zhou, W.; Vajtai, R.; Ajayan, P. M. *Nano Lett.* **2016**, *16*, 1097.
- (18) Sun, M.; Adjaye, J.; Nelson, A. E. *Appl. Catal., A* **2004**, *263*, 131.
- (19) Thomas, R.; van Oers, E. M.; de Beer, V. H. J.; Medema, J.; Moulijn, J. A. *J. Catal.* **1982**, *76*, 241.
- (20) Grange, P. *Catal. Rev.: Sci. Eng.* **1980**, *21*, 135.
- (21) Kibsgaard, J.; Tuxen, A.; Levisen, M.; Laegsgaard, E.; Gemming, S.; Seifert, G.; Lauritsen, J. V.; Besenbacher, F. *Nano Lett.* **2008**, *8*, 3928.
- (22) Le, D.; Sun, D.; Lu, W.; Aminpour, M.; Wang, C.; Ma, Q.; Rahman, T. S.; Bartels, L. *Surf. Sci.* **2013**, *611*, 1.
- (23) Sun, D.; Lu, W.; Le, D.; Ma, Q.; Aminpour, M.; Alcántara Ortigoza, M.; Bobek, S.; Mann, J.; Wyrick, J.; Rahman, T. S.; Bartels, L. *Angew. Chem., Int. Ed.* **2012**, *51*, 10284.
- (24) Grønborg, S. S.; Ulstrup, S.; Bianchi, M.; Dendzik, M.; Sanders, C. E.; Lauritsen, J. V.; Hofmann, P.; Miwa, J. A. *Langmuir* **2015**, *31*, 9700.
- (25) Spanig, A.; Broekmann, P.; Wandelt, K. *Electrochim. Acta* **2005**, *50*, 4289.
- (26) Ling, W. L.; Bartelt, N. C.; Pohl, K.; de la Figuera, J.; Hwang, R. Q.; McCarty, K. F. *Phys. Rev. Lett.* **2004**, *93*, 166101.
- (27) Feibelman, P. J. *Phys. Rev. Lett.* **2000**, *85*, 606.
- (28) Feenstra, R. M.; Stroscio, J. A.; Tersoff, J.; Fein, A. P. *Phys. Rev. Lett.* **1987**, *58*, 1192.
- (29) Lebègue, S.; Eriksson, O. *Phys. Rev. B: Condens. Matter Mater. Phys.* **2009**, *79*, 115409.
- (30) Hilsenbeck, S. J.; McCarley, R. E.; Goldman, A. I.; Schrader, G. L. *Chem. Mater.* **1998**, *10*, 125.
- (31) Benoist, L.; Gonbeau, D.; Pfister-Guillouzo, G.; Schmidt, E.; Meunier, G.; Levasseur, A. *Thin Solid Films* **1995**, *258*, 110.
- (32) Balog, R.; Jorgensen, B.; Nilsson, L.; Andersen, M.; Rienks, E.; Bianchi, M.; Fanetti, M.; Laegsgaard, E.; Baraldi, A.; Lizzit, S.; Slijivančanin, Z.; Besenbacher, F.; Hammer, B.; Pedersen, T. G.; Hofmann, P.; Hornekaer, L. *Nat. Mater.* **2010**, *9*, 315.
- (33) Hornekær, L.; Šljivančanin, Ž.; Xu, W.; Otero, R.; Rauls, E.; Stensgaard, I.; Laegsgaard, E.; Hammer, B.; Besenbacher, F. *Phys. Rev. Lett.* **2006**, *96*, 156104.
- (34) Schmidt, P. K.; Christmann, K.; Kresse, G.; Hafner, J.; Lischka, M.; Groß, A. *Phys. Rev. Lett.* **2001**, *87*, 096103.
- (35) Nørskov, J. K.; Bligaard, T.; Logadottir, A.; Kitchin, J. R.; Chen, J. G.; Pandelov, S.; Stimming, U. *J. Electrochem. Soc.* **2005**, *152*, J23.
- (36) Farias, M. H.; Gellman, A. J.; Somorjai, G. A.; Chianelli, R. R.; Liang, K. S. *Surf. Sci.* **1984**, *140*, 181.
- (37) Lee, J. S.; Lee, K. H.; Lee, J. Y. *J. Phys. Chem.* **1992**, *96*, 362.
- (38) Hammer, B.; Nørskov, J. K. *Nature* **1995**, *376*, 238.
- (39) Nørskov, J. K.; Bligaard, T.; Rossmeisl, J.; Christensen, C. H. *Nat. Chem.* **2009**, *1*, 37.
- (40) Appel, A. M.; Lee, S.-J.; Franz, J. A.; DuBois, D. L.; DuBois, M. *R. J. Am. Chem. Soc.* **2009**, *131*, 5224.
- (41) Appel, A. M.; Lee, S.-J.; Franz, J. A.; DuBois, D. L.; Rakowski DuBois, M.; Birnbaum, J. C.; Twamley, B. *J. Am. Chem. Soc.* **2008**, *130*, 8940.
- (42) Tran, P. D.; Tran, T. V.; Orio, M.; Torelli, S.; Truong, Q. D.; Nayuki, K.; Sasaki, Y.; Chiam, S. Y.; Yi, R.; Honma, I.; Barber, J.; Artero, V. *Nat. Mater.* **2016**, *15*, 640.
- (43) Lin, T.; Shang, X. S.; Adisoejoso, J.; Liu, P. N.; Lin, N. *J. Am. Chem. Soc.* **2013**, *135*, 3576.
- (44) Wang, W.; Shi, X.; Wang, S.; Van Hove, M. A.; Lin, N. *J. Am. Chem. Soc.* **2011**, *133*, 13264.
- (45) Cai, J.; Ruffieux, P.; Jaafar, R.; Bieri, M.; Braun, T.; Blankenburg, S.; Muoth, M.; Seitsonen, A. P.; Saleh, M.; Feng, X.; Mullen, K.; Fasel, R. *Nature* **2010**, *466*, 470.
- (46) Grill, L.; Dyer, M.; Lafferentz, L.; Persson, M.; Peters, M. V.; Hecht, S. *Nat. Nanotechnol.* **2007**, *2*, 687.